This is a repository copy of *Parameterisation methods for piezoelecric transformer equivalent circuit models*.

White Rose Research Online URL for this paper:
https://eprints.whiterose.ac.uk/188639/

Version: Accepted Version

Proceedings Paper:
O'Keeffe, H., Foster, M.P. and Davidson, J.N. orcid.org/0000-0002-6576-3995 (2022) Parameterisation methods for piezoelecric transformer equivalent circuit models. In: 11th International Conference on Power Electronics, Machines and Drives (PEMD 2022). PEMD 2022 - The 11th International Conference on Power Electronics, Machines and Drives, 21-23 Jun 2022, Newcastle, UK (hybrid conference). IET Digital Library , pp. 764-768. ISBN 9781839537189

https://doi.org/10.1049/icp.2022.1152

© 2022 IET. This is an author-produced version of a paper accepted for publication in PEMD 2022. Uploaded in accordance with the publisher's self-archiving policy.

Reuse
Items deposited in White Rose Research Online are protected by copyright, with all rights reserved unless indicated otherwise. They may be downloaded and/or printed for private study, or other acts as permitted by national copyright laws. The publisher or other rights holders may allow further reproduction and re-use of the full text version. This is indicated by the licence information on the White Rose Research Online record for the item.

Takedown
If you consider content in White Rose Research Online to be in breach of UK law, please notify us by emailing eprints@whiterose.ac.uk including the URL of the record and the reason for the withdrawal request.

White Rose
university consortium
Universities of Leeds, Sheffield & York

eprints@whiterose.ac.uk
https://eprints.whiterose.ac.uk/

PARAMETERISATION METHODS FOR PIEZOELECRIC TRANSFORMER EQUIVALENT CIRCUIT MODELS

Henry O'Keeffe[1], Martin P Foster[1], Jonathan N Davidson[1]

[1] *Dept. of Electronic and Electrical Engineering, The University of Sheffield, Sheffield, United Kingdom*

Keywords: RESONANT CONVERTER, MEASUREMENT, MODELLING

Abstract

Three techniques for extracting equivalent circuit parameters from piezoelectric transformers based on the Mason equivalent circuit model are explored, starting from a frequency domain analysis of the input and output impedance. Two optimisation techniques to improve the accuracy of the parameterisation are detailed and tested, each allowing multiple resonant modes to be modelled, with the aim of minimising the percentage error of the fit.

1 Introduction

1.1 Piezoelectric transformers

Piezoelectric transformers (PTs) have uses as alternatives to traditional electromagnetic transformers where low power voltage conversion is required. Electrical energy is converted to mechanical flexing of a piezoelectric material at resonance in the primary section of the device. Since the primary section is mechanically connected to the secondary section, the piezoelectric effect (pressure-to-charge conversion) creates the output voltage.

Due to the resonant operation, high efficiency can be obtained. The lack of reliance on magnetic properties also allows operation of PTs at high temperatures. Commercially, PTs have found uses providing high frequency AC to cold-cathode fluorescent lamps and have found other applications in the space and energy sectors [1].

In the simplest implementation, one piece of piezoelectric material is made with three electrical contacts, one as the input, one common terminal and one output. Depending on the location of the electrical contacts and the geometry of the device, the desired voltage gain can be obtained.

1.2 Equivalent circuit model

To ease design from an electrical perspective, an equivalent circuit model can be used. The simplified Mason equivalent circuit can be seen in Figure 1. Additional parallel branches can be added or removed to account for the desired number of resonant modes.

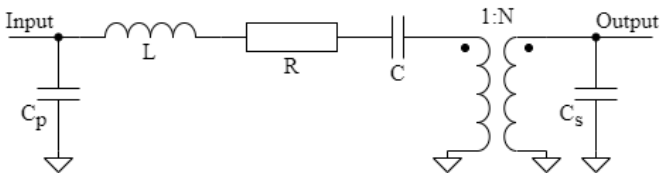

Figure 1 Mason equivalent circuit model

The component values can be obtained by calculation from mechanical properties [2] or by performing electrical measurements of the transformer. The latter is usually more accurate as tolerances associated with the materials specifications and manufacturing processes can be accounted for and, often, it is necessary to confirm calculated results after the PT has been manufactured.

Here, three parameterisation methods are explored: i) a different parameterisation of the cost function employed in [4] provide greater efficacy of the optimiser; ii) the incorporation of an additional step to further refine the parameters and iii) particle swarm optimisation (PSO) where the initial estimates for the equivalent circuit parameters are taken directly from the impedance spectrum.

2 Prior Work

The work presented here builds on that of Horsley, *et al.*, [3] and method 1 from Forrester, *et al*., [4], where the input and output impedance spectra are fitted to the Mason equivalent circuit model shown in Figure 1.

The resonant frequency, $\omega_0 = \frac{1}{\sqrt{LC}}$, of L & C is determined by locating the frequency of minimum impedance measured when the output is connected to the common node (i.e. short-circuited). Specifically, ω_0 is found by evaluating $\min\left|Z_{in(s-c)}(\omega)\right|$ where $Z_{in(s-c)}$ is the impedance looking into the input port of the PT with the output short-circuited (s-c). The resonant frequency provides the product of L and C. The resistance was found as the absolute value of impedance at the resonant frequency, $R \approx Z_{in(s-c)}(\omega_0)$.

Since the output is short-circuited, the effects of C_s and N can be neglected, leaving only C_p and one independent variable from the RLC branch to be determined. Since C_p and the RLC branch are connected in parallel it is difficult to separate them. In [4], a new parameter, β, was introduced to represent the impedance of the RLC branch. Since ω_0 and R have already been determined from the impedance spectrum, only two

variables, C_p and β, need to be obtained from a curve-fit, thereby reducing the search space. The cost function (1) was defined as the mean squared error between the measured impedance ($Z_{reference}$) and the Mason equivalent circuit calculated impedance ($Z_{calculated}$). The summation in (1) is taken over the range of the reference impedance dataset and the $Z_{calculated}$ is determined over the same range.

$$J_1(C_p,\beta) = \sum \left(\frac{|Z_{reference}| - |Z_{calculated}(C_p,\beta)|}{|Z_{reference}|} \right)^2$$

$$\min_{C_p,\beta} J_1(C_p,\beta) \qquad (1)$$

where $Z_{reference} = Z_{in(s\text{-}c)}$. Equation (1) is minimised using the Nelder-Mead method to determine the optimal values for C_p & β. A similar approach can be applied to the output impedance by short-circuiting the input port and measuring the impedance at the output port to provide $Z_{out(s-c)}$. Using $Z_{reference} = Z_{out(s\text{-}c)}$, the optimisation process in (1) can be adapted to extract C_s (in an equivalent manner to C_p) and a referred value for the RLC branch impedance, β', as seen from the output-side which is used to calculate the turn-ratio using $N = \sqrt{\frac{\beta'}{\beta}}$.

To evaluate the performance of the parameterisation, two metrics are used. The metric described (2) is the average absolute error ratio ($E_{\%}$), and (3) describes the average absolute error (E_{abs}).

$$E_{\%} = \frac{\Sigma \left| \frac{|Z_{reference}| - |Z_{calculated}|}{|Z_{reference}|} \right|}{no.\ of\ datapoints} \qquad (2)$$

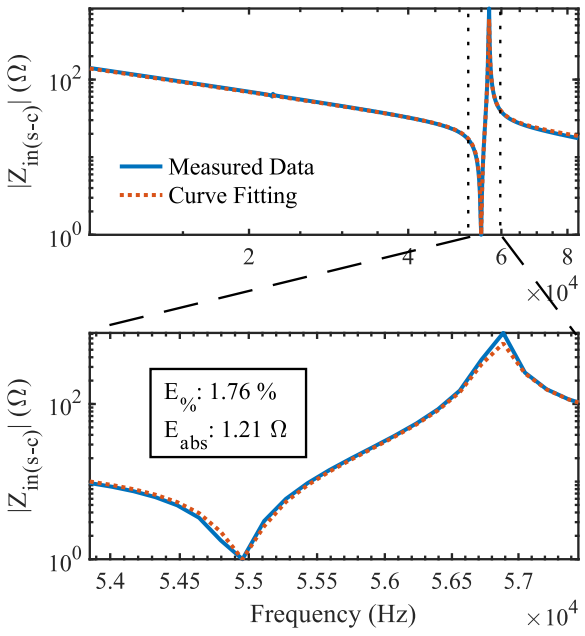

Figure 2 An example curve fit for $|Z_{in(s\text{-}c)}|$

$$E_{abs} = \frac{\Sigma \left| |Z_{reference}| - |Z_{calculated}| \right|}{no.\ of\ datapoints} \qquad (3)$$

To demonstrate this technique, frequency domain impedance data was taken from a STEMiNC SMMTF55P6S50 Rosen PT.

Figure 2 shows a bode plot of the estimated input impedance $|Z_{in(s\text{-}c)}|$ of the PT using the curve fitting technique from [4], along with the measured impedance for comparison.

3 Proposed optimisation techniques

3.1 Technique 1 (T1) - Streamlining for improved convergence

Three independent variables are required to characterise the RLC branch. Method 1 in [4] assumes $\omega_0 L = \frac{1}{\omega_0 C} = \beta$ to link ω_0 to L & C, with R being determined from the impedance spectrum. Since L & C are not known a priori then a large range of β values must be searched to ensure a global minimum can be found. Here, it is proposed that the characteristic impedance β may be substituted by bandwidth or Q-factor (see Figure 3) to give,

$$Q = \frac{f_0}{f_B} = \frac{\omega_0}{\omega_B} = \frac{1}{R}\sqrt{\frac{L}{C}} \qquad (4)$$

where ω_B is the bandwidth and $R \approx Z_0 = Z_{in(s-c)}(\omega_0)$. Using (4) allows the equivalent circuit components to be written as,

$$L = \frac{R}{\omega_B}, \quad C = \frac{\omega_B}{R\omega_0^2} \qquad (5)$$

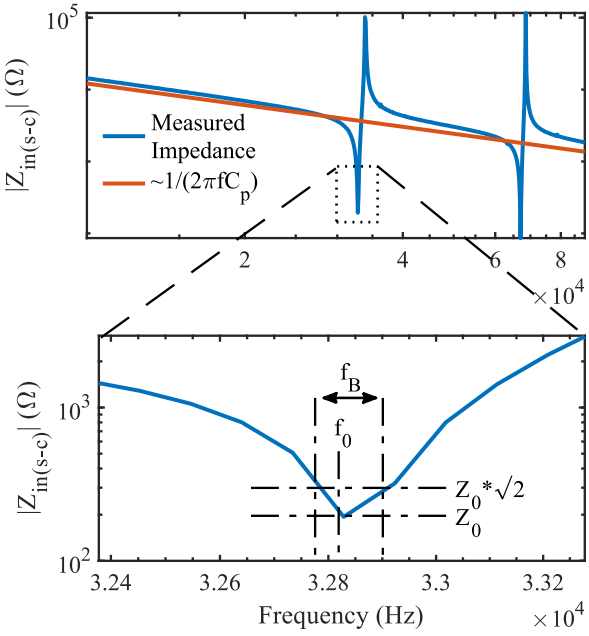

Figure 3 Bandwidth estimation from a bode plot of input impedance

The parameter β in (1) is replaced with ω_B and the optimiser is seeded with an initial value for ω_B extracted from the impedance spectrum, see Figure 3. Taken together, these two steps reduce the search space by a significant factor and act to decouple the interaction between the interdependent variables.

To further improve convergence time an initial estimate for C_p can be found by assuming the low frequency input impedance of the PT is dominated by C_p, as shown by the orange curve in Figure 3. This estimated value is also used to seed the optimiser. When combined, the substitution for ω_B and seeding of the Nelder-Mead minimisation method used in Section 2, reduced total CPU time needed for the fit in Figure 2 from 47 s to 0.9 s.

3.2 Technique 2 (T2) – T1 with pattern search

The success of Technique 1 relies on accurate values for ω_0 and R extracted from the impedance spectrum. It was assumed C_p does not contribute to ω_0 and also that R dominates the impedance at ω_0. Furthermore, T1 only optimises two parameters and therefore cannot correct for any disparity in ω_0 and R. In T2, to improve the fit of the previous technique, a second round of optimisation was done, seeded by the results from T1. All parameters from each impedance spectrum were allowed to be adjusted to provide a global minimum using (2) as the cost function. For this, a pattern search (PS) optimiser was used which is effective for larger search spaces [5].

3.3 Technique 3 (T3) – Particle swarm optimisation (PSO)

In particle swarm optimisation, the term particle refers to a possible solution that exists in both time (iteration) and space (parameter). Multiple particles are initially randomly distributed about the search space. For each iteration, the performance of each particle is evaluated using a cost function, the velocity is updated depending on the lowest cost (error) that that particle obtained in its history, as well as the lowest cost obtained by any other particle. Over time (iterations) the particles converge on the optimal solution traversing the search space [6]. The measured (reference) impedance spectra is fitted to the calculated impedance spectra evaluated using $Z_{in(s\text{-}c)}(C_p, R, \omega_0, \omega_B)$ and $Z_{out(s\text{-}c)}(C_s, N^2R, \omega_0, \omega_B)$. The search space is centred about the initial seed values used by T1 and T2.

3.4 Experimental evaluation of optimisation techniques

All three techniques were tested to determine their performance using same dataset that was used for Figure 2. The T2 (pattern search) used 150 iterations, taking 10 s of CPU time (equivalent time for one core) and 2.5 s of real time. PSO used 300 iterations of 500 particles, taking a CPU time of 1080 s and 45 s of real time (spread over 32 cores). The stopping conditions were chosen by experiment as the point where negligible further improvement was seen, allowing the optimisation techniques the best conditions to perform. The results can be seen in Figure 4.

T3 (PSO) demonstrated the highest performance with this dataset, with a slightly lower percentage error than T1, and a much-reduced absolute error. The superior performance of T3 comes at the cost of requiring more CPU time; approximately 100 times that of T2, and more than 1000 times that of T1 alone. Here, T2 provides a good balance between a reduction in absolute error and processing time.

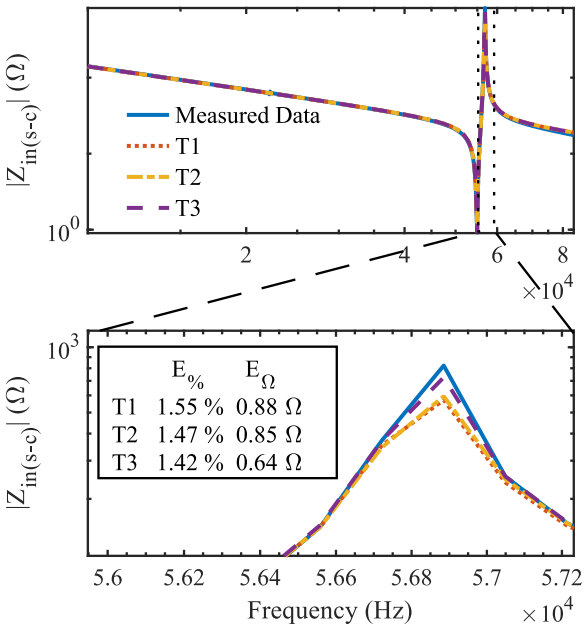

Figure 4 Comparison of curve fitting, curve fitting with pattern search and particle swarm optimisation

4 Multiple Resonant Modes

PT are typically designed to exhibit a strong vibration mode to maximise power transfer and efficiency. However, due to material properties and their geometry PTs exhibit a range of vibration modes and it is useful to quantify these for design and control purposes.

4.1 Modelling multiple resonant modes

The Mason equivalent circuit model in Figure 1 can be extended to account for additional resonant modes by incorporating additional RLC branches. Figure 5 shows an equivalent circuit for modelling k=3 vibration modes.

With reference to Figure 5, when the output port is short-circuited, the input impedance is characterised by the input capacitance connected in parallel with each RLC branch, representing the vibration modes of the mechanical motion. The input impedance can be calculated using (6), where k is the total number of resonant branches to be modelled.

$$Z_{\text{in(s-c)}} = \frac{1}{\mathrm{j}\omega C_p + \sum_{m=1}^{k}\left(R_m + \frac{1}{\mathrm{j}\omega C_m} + \mathrm{j}\omega L_m\right)^{-1}} \tag{6}$$

Similarly, the output impedance is defined by,

$$Z_{\text{out(s-c)}} = \frac{1}{\mathrm{j}\omega C_s + \sum_{m=1}^{k}\left(N_m^2\left(R_m + \frac{1}{\mathrm{j}\omega C_m} + \mathrm{j}\omega L_m\right)\right)^{-1}} \tag{7}$$

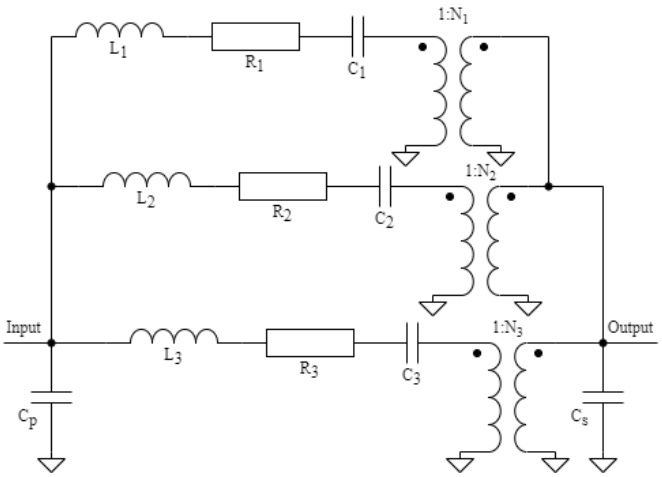

Figure 5 Mason equivalent circuit model with three parallel branches

These equations allow the measured input impedance to be fitted with a model containing $3k + 1$ unknowns. The output impedance was fitted using the concepts applied in T1-3 and the square root of the ratio of the parallel branch impedances seen from either side of the device is the transformer ratio N_m.

4.2 Curve-fitting with multiple branches

The techniques described in section 3 were adapted to parameterise PTs with two active resonant modes. For T1, two curve-fit optimisation runs were performed, with run 1 having the resonant frequency (ω_0), bandwidth (ω_B) and branch resistance (R) at the first vibration mode. Run 2 used values extracted for the second vibration mode. Fixing of ω_0 and R about a vibration mode forces the minimisation algorithm to optimise the impedance error of the resonant branch at that frequency. The RLC values from each run are used to model each branch, with C_p taken as the average of the two.

As described in 3.2, the pattern search T2 operates on all seven parameters ($C_{p/s}$, R_1, L_1, C_1, R_2, L_2 and C_2 or their referred values) simultaneously. T2 was set to halt when the change in cost function was less than 10 ppm per iteration.

To apply T3 described in 3.3 the parameter space needs to be extended to all seven parameters and can be applied using 300 iterations with 500 particles.

4.3 Experimental Results

Seen in Table 1, both T2 and T3 reduce percentage error of the fit compared to T1. The average absolute error follows a similar trend to the percentage error. Table 1 also shows that the CPU time increases dramatically for T2 and T3 when multi-dimensional optimisation is used, with particle swarm optimisation taking several minutes to run on a high-performance system.

The PT has a high series resistance for both resonant branches (R_1 and R_2 in Table 1), which decreases the prominence of the peaks on the impedance plot (Figure 6).

Table 1 Characteristics for the SMMTF85P1S50 PT

Parameter	Technique 1	Technique 2	Technique 3
C_p	30.0 nF	29.1 nF	28.8 nF
C_s	80.6 pF	78.7 pF	75.5 pF
R_1	36.4 Ω	55.5 Ω	97.0 Ω
L_1	4.56 mH	4.73 mH	4.32 mH
C_1	1.02 nF	0.968 nF	1.06 nF
N_1	23.7∠0°	24.3∠0°	19.4∠0°
R_2	16.9 Ω	20.9 Ω	26.0 Ω
L_2	1.08 mH	1.20 mH	1.05 mH
C_2	1.20 nF	1.07 nF	1.24 nF
N_2	26.1∠0°	30.2∠0°	25.2∠0°
$E_{\%(in)}$	4.40 %	1.81 %	2.50 %
$E_{\Omega(in)}$	6.43 Ω	1.06 Ω	1.23 Ω
CPU time	6.9 s	207 s	1770 s

Input and output impedance spectra obtained by measurement and curve-fit are shown in Figure 6 and Figure 7, respectively. All three fitting methods match the resonant frequency with good accuracy, but the T1 alone does not attain a good fit at the first anti-resonant point. T2 improves the agreement at the anti-resonant point. It should be noted that the measured $Z_{out(s\text{-}c)}$ exhibits noise which may have affected the performance of the optimiser.

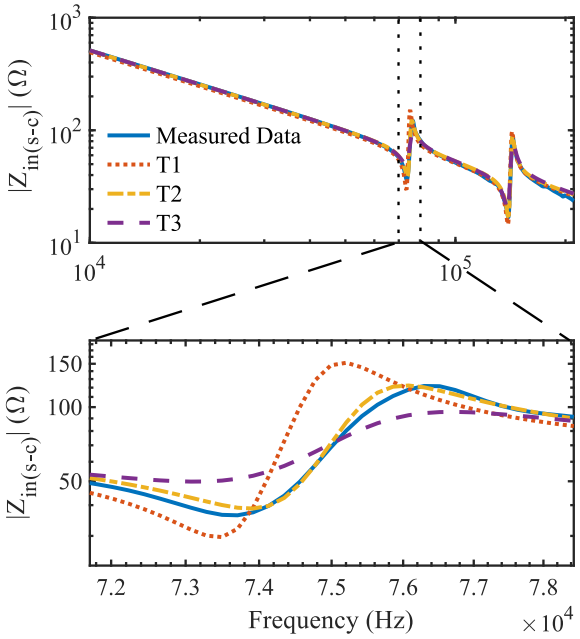

Figure 6 SMMTF85P1S50 PT input impedance

In both figures T3 struggles to capture behaviour about the resonant and anti-resonant frequencies. This behaviour is usually a characteristic of the optimiser becoming trapped in a local minimum and one solution would be to increase the number of particles. It should be noted that increasing the number of particles or iterations is at the cost of a greater processing time of an already computationally intensive method. An efficient remedy could be to seed the positions of the particles directly with values estimated from the impedance spectra.

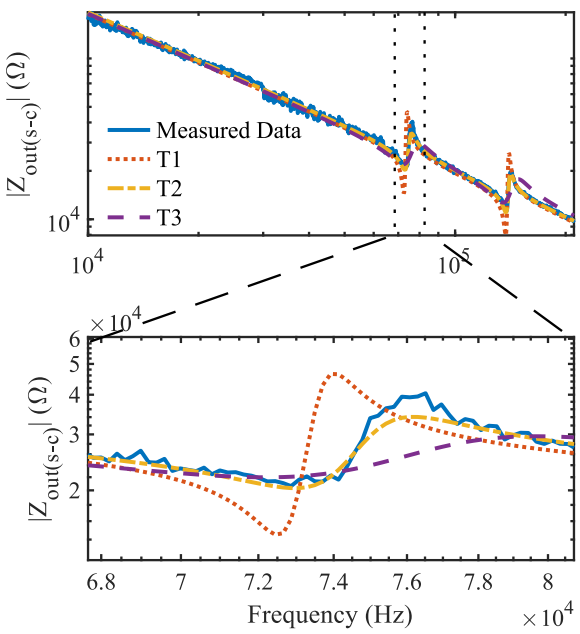

Figure 7 SMMTF85P1S50 PT output impedance

4 Conclusion

An improved version of the curve fitting method has been demonstrated, reducing time taken to parameterise a piezoelectric transformer and extending the parameterisation to multiple resonant modes. Improvements in percentage error have been demonstrated by implementing a pattern search optimisation step after an initial reduced parameter characterisation. Particle swarm optimisation was demonstrated as an alternative, reducing percentage error by approximately a factor of two compared to previously published techniques. In this work the pattern search optimisation technique provided greater performance than PSO while requiring an order of magnitude less CPU time.

5 Acknowledgements

This work has been financially supported by EPSRC: EP/S031421/1.

6 References

[1] A. V. Carazo, "Piezoelectric Transformers: An Historical Review," *Actuators,* vol. 5, no. 2, p. 12, 2016.

[2] Y. Huang, W. Huang, Q. Wang and X. Su, "Research on the Equivalent Circuit Model of a Circular Flexural-Vibration-Mode Piezoelectric Transformer With Moderate Thickness," *IEEE Transactions on Ultrasonics, Ferroelectrics, and Frequency Control,* vol. 60, no. 7, pp. 1538-1543, 2013.

[3] J. Forrester, J. Davidson, M. Foster and D. Stone, "Equivalent Circuit Parameter Extraction Methods for Piezoelectric Transformers," in *21st European Conference on Power Electronics and Applications*, Genova, Italy, 2019.

[4] E. L. Horsley, M. P. Foster and D. A. Stone, "A frequency-response-based characterisation methodology for piezoelectric transformers," in *2nd Electronics System-Integration Technology Conference*, Greenwich, UK, 2008.

[5] C. Audet and J. J.E. Dennis, "Analysis of Generalised Pattern Searches," *SAIM Journal on Optimisation,* vol. 13, no. 3, pp. 889-903, 2003.

[6] J. Kennedy and R. Eberhart, "Particle Swarm Optimisation," in *IEEE International Conference on Neural Networks*, Perth, Australia, 1995.